

ADAPTATION OF AN UNDERWATER ACOUSTIC PROPAGATION MODEL TO INFRASONIC ATMOSPHERIC PROPAGATION

Guy V. Norton and Wayne A. Kinney
Ocean Acoustics Branch, Naval Research Laboratory
Jorge C. Novarini, Planning Systems Inc.
Dan J. Ramsdale, Neptune Sciences, Inc.
Rodney W. Whitaker, Los Alamos National Laboratory

Sponsored by U. S. Department of Energy
Office of Nonproliferation and National Security
Office of Research and Development and
Contract No. DE-AI04-98AL79805

ABSTRACT

For decades, the U. S. Navy has been engaged in the development of underwater acoustic propagation models to aid in the design and effective use of underwater sonar systems. Much of the expertise created in this development is applicable (directly or by modification) to challenges associated with the use of infrasonic arrays to monitor CTBT compliance. We will report on the results of the modification and adaptation of a parabolic-equation underwater propagation model to predict and analyze acoustic-gravity wave signals in both a range-independent and a range-dependent atmosphere. Examples are given that include the effects of range-dependent winds on signal strength for the case of an airborne explosive source and a ground-based infrasonic receiver. Frequencies of interest are in the band from 0.02 to 10 Hz, and ranges of interest are 1000 km or less.

Key Words: infrasound monitoring

1. Introduction

The issues relating to infrasonic propagation in the atmosphere, although long standing, have remained relatively unexplored within the acoustic community. The subject has however acquired renewed interest due to the Comprehensive Test Ban Treaty (CTBT) [1]. Infrasound monitoring is one of the main tools for detecting distant nuclear explosions. The detected signals are the low frequency components (roughly between 0.02 to 10 Hz) of the shock wave produced by an atmospheric nuclear burst. They can be detected at ranges up to a few thousand kilometers by virtue of the waveguide created by ground reflections and refraction in the atmosphere. The problem is essentially that of propagation in a range dependent environment, similar to that occurring in other branches of acoustics. In particular, attention must be given to upper (>10 km) atmospheric winds, the speeds of which can be a significant fraction of the acoustic propagating sound speed [2].

Modeling infrasonic propagation in a realistic environment would provide a useful tool for the test ban treaty monitoring community. However there appears to be a lack of ready-to-use models capable of high fidelity modeling. By high fidelity modeling we mean modeling the propagation of the acoustic energy in an environment which includes all of the nuances and intricacies of the real environment. This would include the range and altitude dependent sound speed due to temperature and density variations, the range and altitude dependent atmospheric winds as well as the range dependent terrain over which the acoustic field propagates. Not only would this range dependent terrain contain variations in such things as density and porosity but also changes in terrain type. Since infrasonic propagation occurs over such large distances, the type of terrain over which the signal propagates could change for example from grassland to forests to mountains, and finally across water. The propagation model should be capable of not only maintaining the correct amplitude (i.e. conserve energy) of the signal but also maintaining the correct phase as it propagates the signal in this complex and dynamic environment.

The underwater acoustic community has, over the years, developed propagation models that are capable of determining the correct amplitude and phase of the acoustic field in very sophisticated and complex environments. These underwater environments are just as complex and dynamic as the atmospheric environments. The propagation models developed are based on a variety of mathematical and physical concepts. The most familiar are those models that solve the reduced wave equation or Helmholtz equation (thus implicitly assuming a point harmonic source i.e. operating in the frequency domain). Among them are; the normal mode solution to the Helmholtz equation; reduction of the Helmholtz equation to a parabolic equation (PE methods); wavenumber integration methods and ray tracing techniques. They each have their strong and weak points. The nearly universal assumption made by each model is that azimuthal coupling is assumed unimportant. The consequence is that the models operate in cylindrical coordinates, assume azimuthal symmetry (i.e. ignore azimuth), which results in a 2-dimensional (r, z) model. When the environment is weakly range-dependent (i.e. the environment does not change rapidly over a short-range interval) the normal mode models give adequate results. If however the environment changes rapidly with range, resulting in mode coupling (energy transferring between modes) then PE models and some wavenumber integration models are more appropriate, since they are marching algorithms and they naturally include the ability to handle range dependence.

This paper is concerned with taking a model, which is widely known to the underwater acoustics community as the split-step Pade' solution of the Finite Element Parabolic Equation (EFEPE) model developed by Collins [3], and adapting it to infrasonic atmospheric propagation. There are PE [4], normal mode and FFP-based [5,6] atmospheric propagation models in the community, with some of them developed specifically for outdoor propagation, such as that of White and Gilbert [4], where a range independent case was analyzed. Other models have their origin in underwater acoustics. In particular, Franke and Swenson [5] and Gudesen [6] have taken well-known underwater acoustic propagation models (FFP and SAFARI) and adapted them to atmospheric propagation. However, none have addressed the infrasonic frequency regime. In this work, several important enhancements to the EFEPE model were incorporated, such as the altitude and range dependent atmospheric winds, as well as a starter appropriate for a point source over a plane reactive interface. The theory behind these additions as well as the theory for PE will be included. Finally, both frequency domain and time domain results will be presented. At the lower end of the frequency range of interest, acoustic gravity waves may play a role. Since the basic

component of the current model (EFEPE) does not account for acoustic gravity waves, they are not included in the current adaptation. Their inclusions will be the subject of future work.

2. Parabolic Equation Theory

The following description is based on the work by Collins [3]. For a more in-depth description, the reader is directed to the original body of work. Recently Lingeitch *et.al.* [7] has developed an acousto-gravity PE. We start with the Helmholtz equation in cylindrical coordinates and assume azimuthal symmetry. Where z is the height above the air-ground interface and r is the horizontal distance from the source located at $r=0, z=z_0$. We assume that $kr \gg 1$ and remove the spreading factor $r^{-1/2}$ from the acoustic pressure p . The PE method is by definition a boundary value problem, thereby requiring that we provide the starting field. In addition, the boundary conditions at the air-land interface (if allowing for geo-acoustic bottom and thus bottom penetration, at the end of the numerical grid) and at the top of the numerical grid (maximum height of the problem). Range dependency is made up through many different range independent regions. In each range-independent region, the acoustic pressure satisfies the farfield equation,

$$\frac{\partial^2 p}{\partial r^2} + \rho \frac{\partial}{\partial z} \frac{1}{\rho} \frac{\partial p}{\partial z} + k^2 p = 0 \quad (1)$$

Where ρ is the density, $k = (1 + i\eta\beta)\omega / c$ is the complex wavenumber, $\eta = (40\pi \log_{10} e)^{-1}$ is the attenuation (in dB per wavelength), c is the sound speed, and ω is the circular frequency. Note that Eq. (1) does not account for gravity waves, this will be handled at a later time. Since $c, r,$ and z depend only on z , Eq. (1) factors as follows:

$$\frac{\partial}{\partial r} + ik_0\sqrt{1+X} \quad \frac{\partial}{\partial r} - ik_0\sqrt{1+X} \quad p = 0, \quad (2)$$

$$X = k_0^{-2} \rho \frac{\partial}{\partial z} \frac{1}{\rho} \frac{\partial}{\partial z} + k^2 - k_0^2, \quad (3)$$

where c_0 is the reference sound speed and $k_0 = \omega / c_0$. The following approximation is valid if the outgoing component of p dominates the incoming component:

$$\frac{\partial p}{\partial r} = ik_0\sqrt{1+X} p. \quad (4)$$

Removing the factor $\exp(ik_0r)$ from p , we obtain

$$\frac{p}{r} = ik_0 \left(-1 + \sqrt{1+X} \right) p. \quad (5)$$

To obtain the split-step Pade' solution, Eq. (5) is solved analytically before applying a Pade' approximation. Given the field over z at an arbitrary range r , the solution of Eq. (5) at the range $r + \Delta r$ is

$$p(r + \Delta r) = \exp[i\sigma \left(-1 + \sqrt{1+X} \right) \Delta r] p(r) \quad (6)$$

where $\sigma = k_0 \Delta r$. Now imposing a Pade' approximation to the RHS of Eq. (6) we obtain,

$$\exp[i\sigma(-1 + \sqrt{1 + X})] \left[1 + \prod_{j=1}^n \frac{a_{j,n} X}{1 + b_{j,n} X} \right] \quad (7)$$

Substituting Eq. (7) into Eq. (6), we obtain the split-step Pade' solution,

$$p(r + \Delta r) = p(r) + \prod_{j=1}^n a_{j,n} \left(1 + b_{j,n} X \right)^{-1} X p(r) \quad (8)$$

The depth operator is discretized-using finite-differences. The resulting matrices are tridiagonal.

3. Modification of the basic PE model

There are four major changes made to EFEPE resulting in the atmospheric version (Air-EFEPE). First the sound speed is complex through the entire vertical extent of the problem. Second, the starting field incorporated is based on the reflection of a spherical wave from a locally reacting boundary. Third, the inclusion of altitude dependent atmospheric winds, and lastly a new bottom boundary condition is imposed. For an in depth discussion of each modification the reader is directed to a paper by Norton *et al.* [8]. However since the effect of wind is examined by an example, the method of including wind into the model will be presented.

Atmospheric Winds

For the model under consideration, any environmental effect in the fluid mass (atmosphere) has to be included through the index of refraction. However, the wind is a directional phenomenon while temperature (main parameter controlling the sound velocity) is a scalar. Therefore, wind speed cannot be simply added to the local sound speed. A more rigorous approach is required. Nijs and Wapenaar [9] treated the wind speed as a vector quantity resulting in a modified propagation wavenumber. Assuming air to be an ideal gas and sound propagation to be an adiabatic process, one can write, $K = \gamma P_0$, where P_0 is the static pressure, and $\gamma = C_p/C_v$ (the ratio of the specific heats). With these assumptions, the wavenumber can be rewritten. Introducing the Mach vector \mathbf{m} (which is altitude dependent), we have

$$c^2 = \gamma P_0 / \rho_0 \quad (9a)$$

$$m_x = w_x / c, \text{ and } m_y = w_y / c, \quad (9b)$$

$$k = \omega / c, \quad (9c)$$

$$k_m = \omega / c - m_x k_x - m_y k_y. \quad (9d)$$

The local wind speed c incorporates the effects of temperature while \mathbf{m} stands for the wind effect. The first variable is a scalar and the second is a vector. w_x and w_y denote the local wind speed. The wavenumber k of Eq. (9c) is now replaced by k_m of Eq. (9d). Now a determination of k_x and k_y is required. k_x and k_y are the horizontal components of the wavenumber in the x and y direction. Since PE is a 2-Dimensional model (range and altitude) k_x and k_y have the following description,

$$k_x = k \frac{\frac{P}{r}}{\sqrt{\frac{P}{r}^2 + \frac{P}{z}^2}} \cos(\theta) \quad k_y = k \frac{\frac{P}{r}}{\sqrt{\frac{P}{r}^2 + \frac{P}{z}^2}} \sin(\theta) \quad (10)$$

where θ is the angle that r makes to the x-axis. The derivative of p with respect to z is performed using a central difference stencil, while the derivative with respect to r utilizes a backward difference stencil, which requires saving the pressure at the previous range.

To reduce the execution time, the model is parallelized via use of the “DOACROSS” commands available on Silicon Graphics Incorporation (SGI) multi-processor platforms.

4. Examples

Two examples will be presented showing some of the capabilities of the model. The first example shows a time domain result for the propagation of the infrasonic pulse resulting from a nuclear explosion in the atmosphere. The environment for this case is very simple. The sound speed is constant with height (300 m/s) and there are no winds. The source location is at a height of 5 m with the receiver location at a height of 1 m. The model was run for 140 frequencies starting at a frequency of .05 Hz, with a frequency increment of .05 Hz. Initially each frequency had equal weighting. A pressure signature commonly used to investigate the excitation of infrasonic modes by nuclear explosions is the so-called Glasstone pulse [10]. It represents the pressure history of the blast wave. It has the form

$$\frac{p_G(t)}{p_{ref}} = 1 - \frac{t}{T_+} e^{-(t/T_+)} U \left(\frac{t}{T_+} \right), \quad (11)$$

with

$$T_+ = 0.33 \left(1 + 0.047 \ln \frac{R}{R_{ref}} \right)^{1/2} \quad (12)$$

and t is measured from the onset of the shock. $U(*)$ is the Heaviside step function. The parameter p_{ref} is the shock overpressure at a reference distance R_{ref} from a 1KT burst in the standard atmosphere. The shock overpressure at a reference distance of 5.84 R_{ref} , (where $R_{ref} = 256\text{m}$) is 34mbar. The spectral amplitude for the Glasstone pulse is given by

$$A_G(\omega) = \frac{-i}{2\pi \left(i\omega - \frac{1}{T_+} \right)^2} \quad (13)$$

For each frequency, since we are dealing with a cw model, weights determined from Eq. (13) were applied to the output of Air-EFEPE. The resulting time signal is then obtained via an inverse FFT. Figure 1 depicts the comparison of the Air-EFEPE model along with the Glasstone pulse at a range of 1000km. The widths of the two pulses are approximately the same as are the over pressure and role-off. The main difference is that the Glasstone pulse does not show the large over pressure excursion that the synthesized signal does. The reason for the difference was believed to be due to the fact that the analytic expression for the Glasstone pulse knows nothing about the source receiver geometry or about the complex impedance of the land. Therefore, a simplified expression for the pressure near grazing, based on work by Attenborough [11], was used to synthesize a signal. This signal was compared to the Air-EFEPE result. Figure 2 depicts the comparison. Note that the widths of the two signals are a better match than that shown in Fig. 1a. The overpressure that occurs after the large negative excursion does not compare as well as the Glasstone pulse did. However there is an overpressure occurring prior to this negative excursion. It is not as large as the synthesized signal but this could be due to the fact that it is an approximate solution.

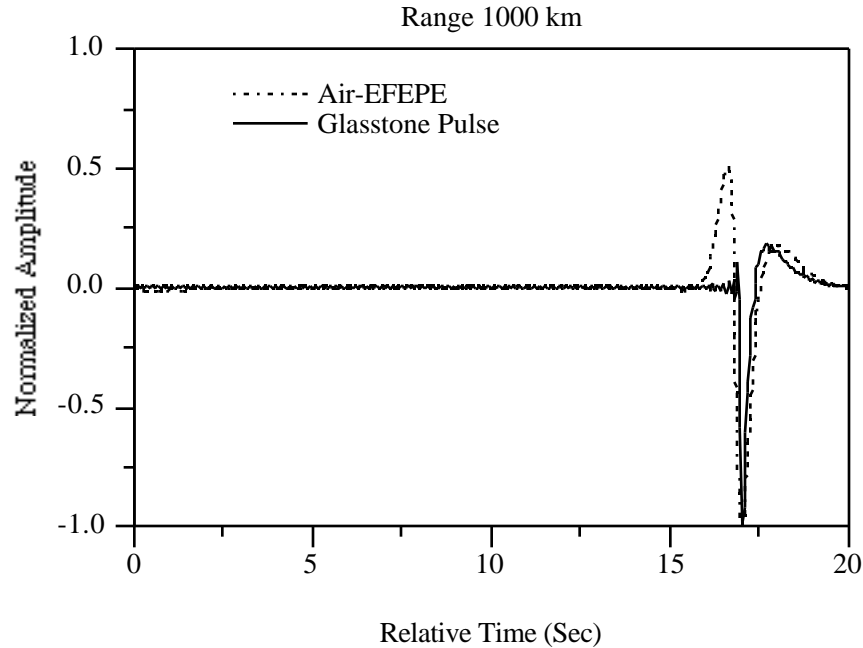


Figure 1. Comparison of the pulse generated by the Air-EFEPE model and the analytic expression for the Glasstone pulse.

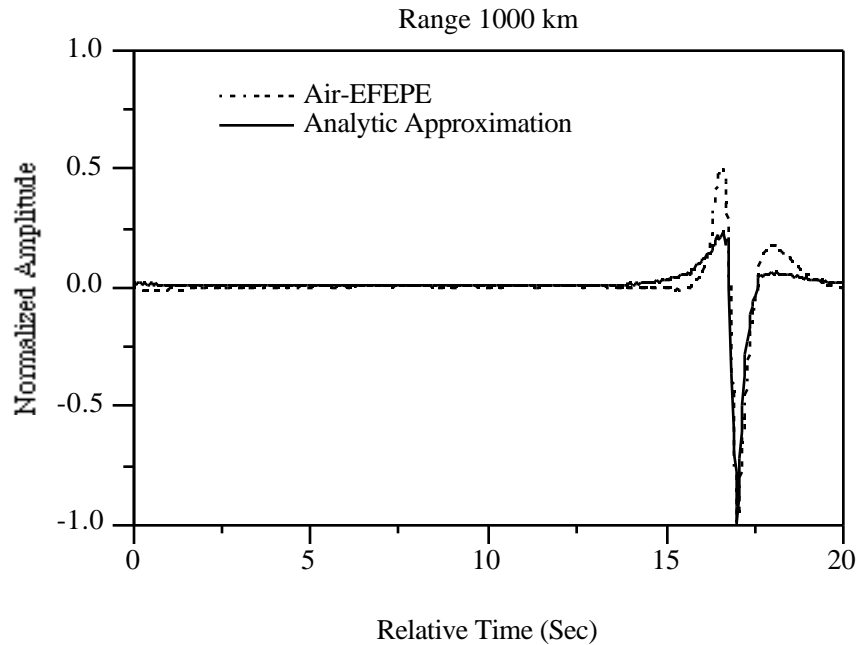


Figure 2. Comparison of the pulse generated by the Air-EFEPE model and the analytic approximation for the pulse from Attenborough.

The second example depicts a frequency domain result. This example is not meant to be realistic. It is used to show that range dependence is included for both sound speed and atmospheric winds. The environment initially consists of an isovelocity sound speed (330 m/s) from the ground to an altitude of 300 km. A 5 Hz source is placed at 150 km. Five separate cases were run. For the first case the environment did not change with range, or in other words this represents a range independent case. This case was run so that the results from the next four cases could be compared to this range independent (baseline environment) environment. Figure 3 depicts the result.

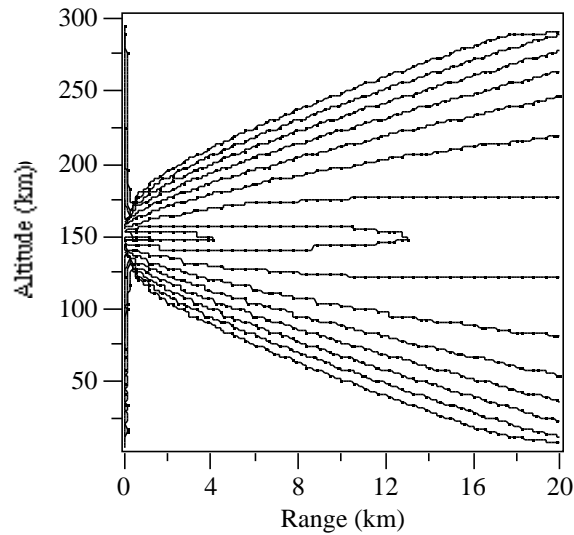


Figure 3. Contour plot of the acoustic field, altitude vs. range for the isovelocity sound speed. Contour levels are 30 to 150 dB in steps of 10 dB.

The sound speed varies with range for the second environment. For this case the sound speed had a minimum at 150 km, while the sound speed at the surface and at 300 km remains at 330 m/s. This minimum becomes more extreme at each kilometer out to 10 km where the minimum is 180 m/s. Beyond 10 km the minimum sound speed reverses until at 20 km the sound speed is once again isovelocity (constant 330 m/s). This results in a sound speed gradient that increases with range, to 10 km and then reverses until at 20 km the gradient disappears. The change in the minimum sound speed is 15 m/s at every km. See Fig. 4 for the resulting sound speed profiles.

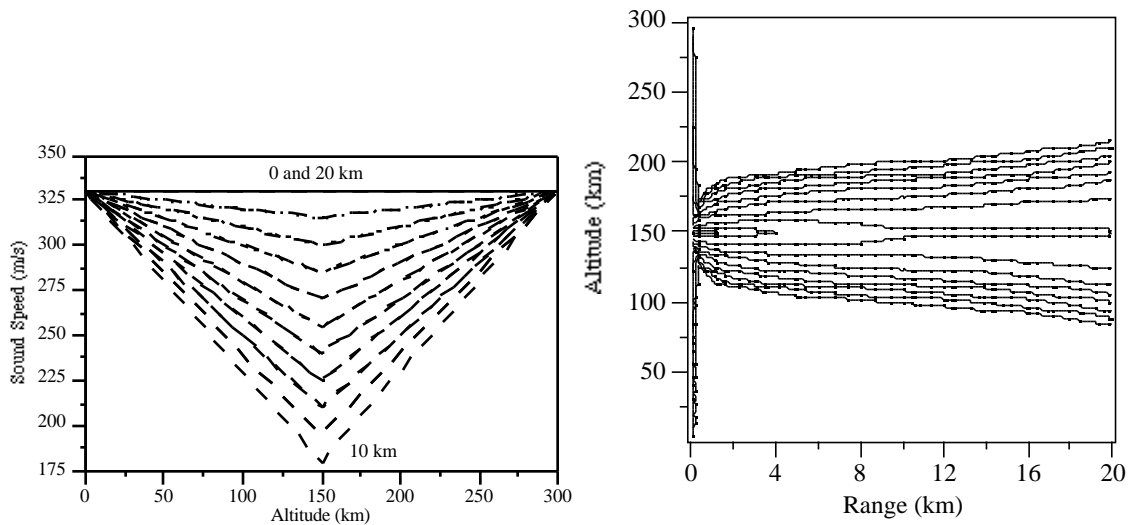


Figure 4a. Sound speed profiles for environment 2. Figure 4b. Contour plot of the acoustic field, altitude vs. range for the 2nd environment (sound speed shown in Fig. 4a). Contour levels are 30 to 150 dB in steps of 10 dB.

Figure 4b depicts the intensity of the acoustic field (expressed in dB) versus altitude and range. Notice that compared to the isovelocity case (Fig. 3) the field is very focused. This is the result of the sound speed gradients. From 10 km to 20 km the strengths of the gradients become less, resulting in a gradual spreading of the acoustic field.

The sound speed profiles used for the 3rd environment are depicted in Fig. 5a. Now instead of having a minimum at an altitude of 150 km there is a maximum. At each kilometer in range, starting at 1 km the maximum increases at a rate of 15 m/s out to 10 km (Maximum sound speed is 480 m/s). From 11 km to 20 km in range the maximum decreases by 15 m/s at each kilometer, until at 20 km the sound speed is once again constant (330 m/s). See Fig. 5a.

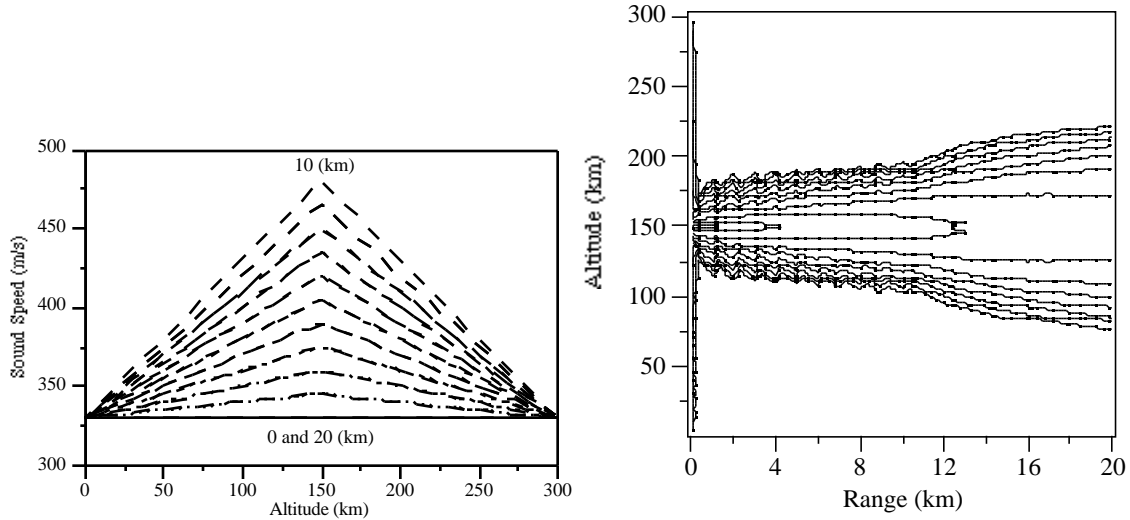


Figure 5a. Sound speed profiles for environment 3. Figure 5b. Contour plot of the acoustic field, altitude vs. range for the 3rd environment (sound speed shown in Fig. 5a). Contour levels are 30 to 150 dB in steps of 10 dB.

Figure 5b depicts the result for this environment. Notice that this result is significantly different from the last result and from the isovelocity result (Fig. 3). The field is very focused and there appears to be some symmetric structure out to 10 km. This structure is due to the fact that the gradient increases only at discrete ranges (and remaining constant until the next increase) and not continuously with range. After 10 km the strengths of the gradients decrease, allowing the acoustic field to spread in height.

The next two environments consist of an isovelocity sound speed (330 m/s) with a range dependent atmospheric wind field. The wind speed profiles used for the 4th environment is depicted in Fig. 6a. This environment is similar to environment 2 (Fig. 4a) except the wind speed x-axis component (at 150 km height) increases in the negative x direction. At each kilometer in range, starting at 1 km the wind speed increases at a rate of 15 m/s out to 10 km (Maximum wind speed is 150 m/s in the negative x direction). From 11 km to 20 km in range the wind speed decreases by 15 m/s at each kilometer, until at 20 km the wind speed is once again constant (0 m/s). See Fig. 6a.

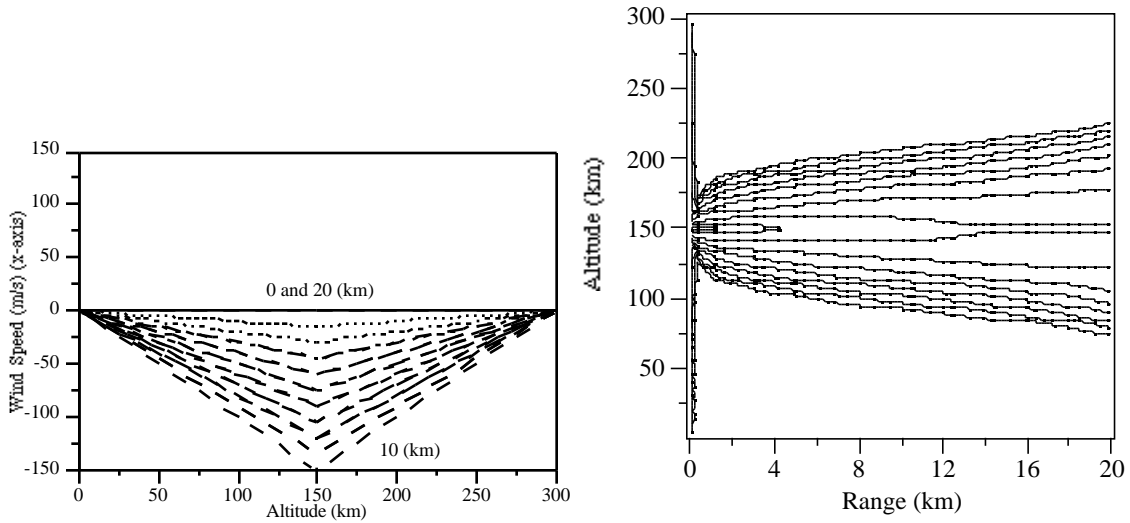


Figure 6a. Wind speed profiles used in 4th environment. Figure 6b. Contour plot of the acoustic field, altitude vs. range for the 4th environment (wind speed shown in Fig. 6a). Contour levels are 30 to 150 dB in steps of 10 dB.

Figure 6b depicts the intensity of the acoustic field (expressed in dB) versus altitude and range. Notice that compared to the results from first environment (Fig. 4b) the two are nearly identical. The differences are noticeable at the maximum range, where field has spread out more in height than when the sound speed changed. This result is not surprising, since the act of changing the local sound speed, results in a change of the local wavenumber, whereas including the wind field results in a direct change of the wavenumber while not changing the sound speed. Again we see that from 10 km to 20 km the strengths of the gradients become less, resulting in a gradual spreading of the acoustic field.

The wind speed profiles used for the 5th environment is depicted in Fig. 7a. This environment is similar to environment 3 (Fig. 5a) except the wind speed x-axis component (at 150 km height) increases in the positive x direction. At each kilometer in range, starting at 1km the wind speed increases at a rate of 15 m/s out to 10 km (Maximum wind speed is 150 m/s in the positive x direction). From 11 km to 20 km in range the wind speed decreases by 15 m/s at each kilometer, until at 20 km the wind speed is once again constant (0 m/s). See Fig. 7a.

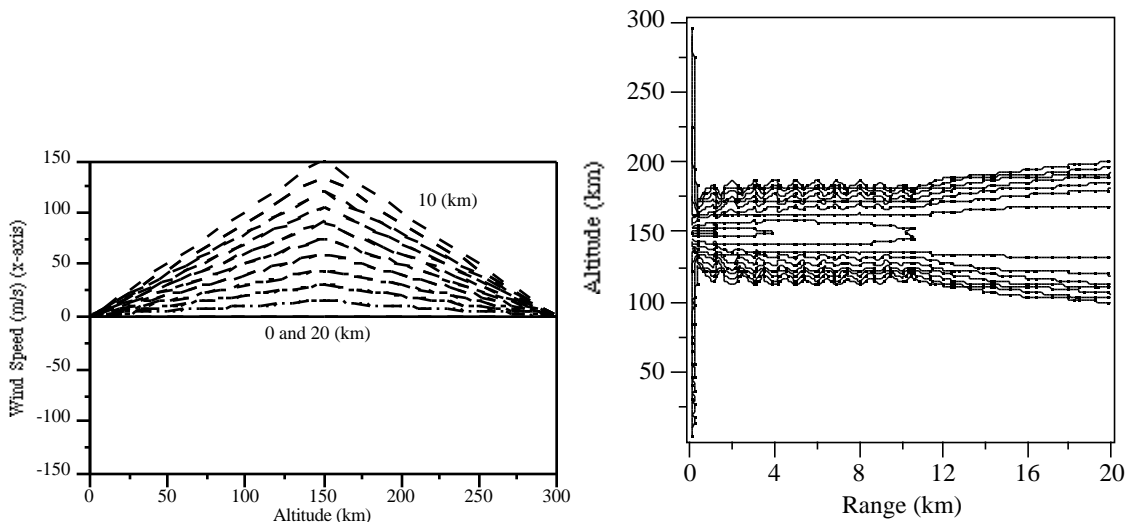


Figure 7a. Wind speed profiles used in 5th environment. Figure 7b. Contour plot of the acoustic field, altitude vs. range for the 5th environment (wind speed shown in Fig. 7a). Contour levels are 30 to 150 dB in steps of 10 dB.

Figure 7b depicts the intensity of the acoustic field (expressed in dB) versus altitude and range. Notice that compared to the results from 3rd environment (Fig. 5b) the two again are nearly identical. Differences are noticeable throughout the range of propagation. The reason is again due to the fact that changing the local sound speed, results in a change of the local wavenumber, where as including the wind field results in a direct change of the wavenumber while not changing the sound speed. It is apparent that the field is more focused in range compared to Fig. 5b.

5. Concluding remarks

A prototype atmospheric acoustic propagation model for infrasonics has been introduced whose genesis is in underwater acoustic propagation. This prototype model includes range and altitude dependent atmospheric winds, and accounts for attenuation in the atmosphere. A starting field is incorporated based on the reflection of a spherical wave from a locally reacting boundary, and lastly a new bottom boundary condition appropriate for an air-ground interface is imposed. The inclusion of the gravity term in the wave equation will be the subject of future work.

Acknowledgements

This work was sponsored by the U. S. Department of Energy and the Los Alamos National Laboratory under contract No. DE-AI04-98AL79805.

References

- [1] Sullivan, J. D., "The Comprehensive Test Ban Treaty," (March 1998), *Physics Today*, 24-29.
- [2] Whitaker, R. W., "Infrasonic Monitoring," 1995, Phillips Laboratory Monitoring Symposium, Scottsdale, Arizona, USA.
- [3] Collins, M. D., "A split-step Pade' solution for the parabolic equation method," *J. Acoust. Soc. Am.*; 1993, **93**, 1736-1742.
- [4] White, M. J., Gilbert, K. E., "Application of the parabolic equation method to the Outdoor Propagation of Sound," *Applied Acoustics*, 1989; **27**, 227-238.
- [5] Franke, S. J., Swenson, Jr. G. W., "A brief tutorial on the Fast Field Program (FFP) as applied to sound propagation in the air;" *Applied Acoustics*, 1989, **27**, 203-215.
- [6] Gudesen, A., "Application of the SAFARI model to sound propagation in the atmosphere," *J. Acoust. Soc. Am.*; 1990, **87**, 1968-1974.
- [7] Lingeitch, J. F., Collins, M. D. and Siegmann, W. L., "Parabolic equations for gravity and acousto-gravity waves," *J. Acoust. Soc. Am.*; 1993, **105**, (6) 3049-3056.
- [8] Norton, G. V. and Novarini, J. C., "Modeling infrasonic atmospheric propagation via a finite element parabolic equation model," submitted to *Applied Acoustics*.
- [9] Nijs, L., Wapenaar, C. P. A., "The influence of wind and temperature gradients on sound propagation, calculated with two-way wave equation," *J. Acoust. Soc. Am.*; 1990, **87**, 1987-1998.
- [10] Posey, J. W., Application of Lamb Edge Mode Theory in the Analysis of Explosively Generated Infrasound, Ph. D. Thesis, Department of Mechanical Engineering, Massachusetts Institute of Technology, Cambridge, MA, August 1971.
- [11] Attenborough, K., Review of ground effects on outdoor sound propagation from continuous broadband sources, *Applied Acoustics*; 1988, **24**, 289-319.